

Contents lists available at ScienceDirect

Journal of the Mechanics and Physics of Solids

journal homepage: www.elsevier.com/locate/jmps



A multiscale chemomechanics theory for the solvent – Assisted recycling of covalent adaptable network polymers



Xiaojuan Shi^{a,b}, Drake Soule^a, Yiqi Mao^c, Christopher Yakacki^a, Haibao Lu^{b,*}, Kai Yu^{a,*}

- ^a Department of Mechanical Engineering, University of Colorado Denver, Denver, CO 80217, USA
- ^b National Key Laboratory of Science and Technology on Advanced Composites in Special Environments, Harbin Institute of Technology, Harbin 150080, PR China
- ^c College of Mechanical and Vehicle Engineering, Hunan University, Hunan 410006, PR China

ARTICLE INFO

Article history: Received 28 October 2019 Revised 28 January 2020 Accepted 26 February 2020 Available online 3 March 2020

Keywords:
Covalent adaptable network polymers
Bond exchange reactions
Solvent-assisted recycling
Chemomechanics theory
Multiscale modeling

ABSTRACT

Thermosetting polymers are hard to be recycled using conventional methods due to their permanently crosslinked networks. It was recently reported that covalent adaptable network (CAN) polymers could be fully decomposed in organic solvents utilizing bondexchange reactions (BERs). Re-polymerization occurs by heating the decomposed solution to evaporate the solvent. This prominent feature of CANs provides exciting opportunities to enable the green and sustainable recycling of thermosets. In this paper, we develop a multiscale chemomechanics theory to study the re-polymerization process of CANs, where the soluble chain segments connect at the tails via BERs. At the macromolecular level, the chemical reaction rates are formulated by considering the distance and diffusivity of reactive species, which determine the average chain segment length and network degree of curing (DoC). The evolution rule of DoC is then fed into the continuum-level multibranched model to capture the thermomechanical properties of CANs at different curing states. The established theory can predict the conversion ratio of functional groups, solution viscosity, volume shrinkage, and glass transition behaviors of re-polymerizing CANs. It also reveals the influencing mechanisms of various material and processing conditions, which paves the road for the immediate engineering applications of the green and sustainable recycling approach for thermosets and their composites.

© 2020 Elsevier Ltd. All rights reserved.

1. Introduction

Conventional thermosetting polymers cannot be reshaped or recycled after polymerization due to their permanently crosslinked networks, which lead to a significant amount of waste materials that end up in landfills and incineration (Hartt and Carey 1992; Kouparitsas et al. 2002; Conroy et al. 2006; Pickering 2006; Ogi et al. 2007; Palmer et al. 2009). The recently emerged covalent adaptable network (CAN) polymers provide exciting opportunities for thermoset reprocessing and recycling. These polymers are covalently crosslinked, but the dynamic nature of reversible bonds allows the network rearrangement through bond-exchange reactions (BERs), where an active unit replaces a unit in an existing bond to form a new bond (Adzima et al. 2008; Kloxin et al. 2010; Tasdelen 2011; Wojtecki et al. 2011; Bowman and Kloxin 2012). When such

E-mail addresses: luhb@hit.edu.cn (H. Lu), kai.2.yu@ucdenver.edu (K. Yu).

^{*} Corresponding authors.

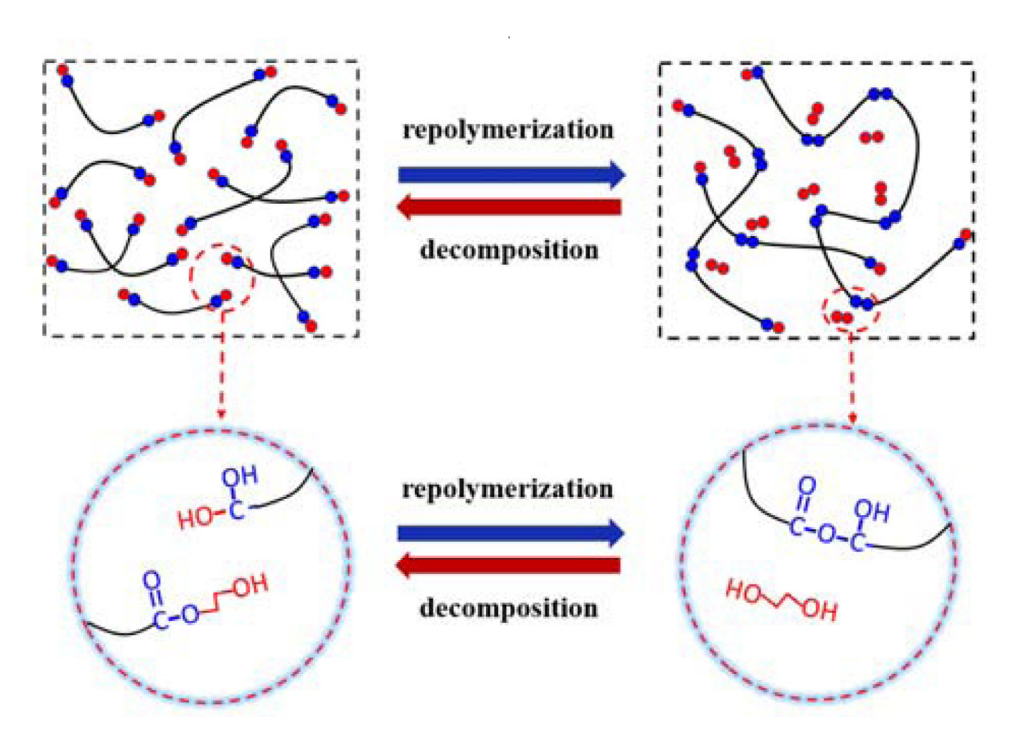


Fig. 1. The re-polymerization of epoxy vitrimer decomposed by the ethylene glycol solvent.

macromolecular events occur in large amounts, they can attribute to unusual properties that are not seen in conventional thermosetting polymers, such as thermoforming (Scott et al. 2005; Scott et al. 2006; Park et al. 2010; Hanzon et al. 2017; Luo et al. 2018a, 2018b, 2019), self-healing (Chen et al., 2003; 2002; Zhang et al. 2009; He et al. 2018), and reprocessing (Taynton et al. 2014; Yu et al. 2014).

A green and sustainable recycling method of thermosets can be realized by leveraging the interactions between CANs and reactive solvent. When a CAN sample is immersed in a suitable organic solvent, solvent molecules diffuse into the network and participate in BERs with exchangeable bonds on the chain backbone, which effectively break the chains into short segments and eventually decompose the network. The choice of solvent depends on the dynamic chemistry employed in the CANs. For example, CANs containing dynamic disulfide bonds can be decomposed in thiol-containing solvents (Johnson et al. 2015; Luzuriaga et al. 2016). Polyimine with imine exchange reactions can be degraded in diamine solvents (Taynton et al. 2016; He et al. 2019). Epoxy vitrimers with transesterification-type BERs can be decomposed in an alcohol solvent (Yu et al. 2016; Shi et al. 2017; Shi et al. 2018). Re-polymerization can occur by heating the decomposed CAN solution in an open environment to evaporate the solvent. The re-polymerization process of the epoxy vitrimer after decomposing in the ethylene glycol (EG) solvent is shown in Fig. 1: at the high temperature, BERs between the exchangeable groups at the end of chain segments connect them together. As the generated solvent molecules evaporating out, the average chain segment length and molecular weight increase, and the polymer network is gradually formed. Fourier transform infrared spectroscopy (FTIR) and mechanical tests confirmed that the recycled epoxy had nearly-identical network structure and mechanical properties as unprocessed ones. The elastic modulus and strength of the recycled materials were about 98.3% and 93.3%, respectively, of the unprocessed samples (Taynton et al. 2016).

The solvent-assisted recycling method of CANs involves simple heating in the organic solvent and realizes full recyclability with low cost, easy implementation, and zero pollution. It represents a paradigm shift away from traditional views of thermoset recycling. However, due to its nascent development, existing studies mainly focused on proof-of-concept demonstrations. There is no systematic experimental or theoretical work that has been performed to address the fundamental questions. For example, what is the relationship between BER kinetics and the evolution of network structure, volume shrinkage, and mechanical properties of the re-polymerizing network? What are the influences of various material and process parameters on the recycling performance? The lack of fundamental understanding prevents the immediate engineering applications of the solvent-assisted recycling method.

The polymerization process of thermosetting polymers has been intensively studied before, but existing modeling theories are insufficient to understand the solvent-assisted recycling process of CANs. First, the theories usually describe the kinetics of chemical reactions (e.g. the step-growth and chain-growth reaction) using empirical mathematics models (Buback et al. 1994, Lee et al. 2001, Atai and Watts 2006, Dickey and Willson 2006, Long et al. 2009). A constant reaction rate is assumed, which is determined by fitting with the experimental data. However, during the CAN re-polymerization, the reaction rates of chain cleavage and connection are governed by the content, relative distance, and diffusivity of

Fig. 2. Structures of the chemical reagents used in this study.

reactive species (i.e. the polymer chains and solvent molecules), which evolve with the polymerization degree. To this end, physics-based constitutive relations based on these governing factors should be defined to study the CAN re-polymerization, which are more effective to identify the influencing mechanism of different material properties and processing conditions, such as the temperature, network crosslinking density, choice of organic solvent, and BER catalyst content. In addition, existing studies primarily focus on the network equilibrium properties during polymerization, such as the increment of Young's modulus. There is a lacking of efficient theory to link the macromolecular-level BER kinetics to the evolution of macroscopic thermo-viscoelastic properties of re-polymerizing thermosets.

In this paper, a multiscale chemomechanics modeling framework is developed to study the evolution of network structure and material properties during the re-polymerization process of CANs. In the microscale, the BER kinetics is formulated by considering the average distance and diffusivity of solvent molecules and chain segments. Statistical analysis of the chemical reactions identifies the distribution of chain segment length and the evolution of functional groups. A degree of conversion (DoC, varies from 0 to 100%) of functional groups is then defined to link the microscale reaction process with macroscopic material properties, such as the volume shrinkage and the evolution of resin viscosity. The DoC is used as an internal variable and fed into a continuum-level multi-branched model to describe the evolution of network thermo-viscoelastic properties during the re-polymerization, including the glass transition temperature and storage modulus. The multiscale chemomechanics theory is verified by corresponding experiments. It is further applied to perform parametric studies to examine the influences of BER catalyst content, choice of solvent, and network crosslinking density on the re-polymerization rate. Compared to existing works, the developed modeling framework integrates the microscale BER kinetics to the continuum-level network thermomechanical properties. It has two major innovations. First, the microscale reaction kinetics is formulated based on the content, relative distance, and diffusivity of reactive species (exchangeable bonds and solvent molecules), instead of following existing works that use constant reaction rate fit with experimental data. The physics-based constitutive relations provide the opportunity to study the influences of various material and processing conditions. Second, the microscale statistical analysis of chemical reactions and chain length distribution is linked to a continuum-level thermomechanical model, which is able to capture the viscoelastic effects, glass transition behaviors, and evolution of network equilibrium modulus during the re-polymerization of CANs. Overall, the presented study advances the understanding of the structural-processing-property relationships of thermosets during the re-polymerization. It also provides valuable guidelines to select the solvent and processing conditions for efficient recycling of thermosets and their composites, which pave the road for the immediate engineering applications of the green and sustainable recycling method.

2. Materials and experiments

2.1. Material synthesis

The material used in this study is the thermosetting epoxy polymer developed by Leibler and coworkers [16]. The epoxy samples were synthesized from the monomer diglycidyl ether of bisphenol A (DGEBA, Sigma Aldrich, St. Louis, MO), the crosslinker fatty acids (Pripol 1040, Croda Inc., Houston, TX), and the metallic BER catalyst (Zn (Ac)₂, Sigma Aldrich). Detailed chemical structures of each reagent are shown in Fig. 2. For polymer synthesis, the catalyst was first mixed with the fatty acid (10 mol% to COOH groups) in a beaker. The temperature was gradually increased from 100 to 150°C while maintaining

Fig. 3. Chain cleavage and chain connection reactions during the network decomposition and re-polymerization.

the mixture under vacuum until no gas evaporation was observed, and the catalyst particles were completely decomposed (3 h). DGEBA was then added to the previous fatty acid mixture containing solubilized catalyst (stoichiometry between fatty acid and epoxy is 1:1) in a round-bottom flask and manually stirred at 130°C until the mixture became homogeneous. Finally, the mixture was poured into a mold and cured in an oven for six hours at 130°C.

2.2. Network decomposition and re-polymerization

The mechanism of chain connection and cleavage during the network decomposition and re-polymerization of epoxy is shown in Fig. 3. The synthesized epoxy vitrimers contain ester groups on the chain backbone. During the decomposition, epoxy samples were immersed in 180°C EG solvent, and the container was sealed to avoid solvent evaporation. The solvent molecules gradually diffused into the network and broke the polymer chains at the positions of ester groups on the backbone. The mole ratio between the EG solvent and epoxy was set to be 1:1 such that the polymer was fully decomposed into unit segments, and there was negligible EG solvent left in the solution.

During the re-polymerization, the decomposed polymer solution was poured into a mold and heated at a given temperature in an open environment. The BERs proceeded stepwise between short segments by combining their functional groups at the end, which form long polymer chains and EG molecules. Crosslinking networks were gradually formed as the EG molecules evaporated out.

2.3. Fourier transform infrared spectroscopy measurement

The decomposed polymer solution was respectively heated at 160, 180, and 200°C for different times for repolymerization. Fourier transform infrared spectroscopy (FTIR) tests were then conducted to monitor the conversion of hydroxyl groups during the epoxy re-polymerization, which has a characteristic peak at 3500–3700 cm⁻¹ (Montarnal et al. 2011). The FTIR measurements were performed by using a spectrometer (Nicolet iS50 FTIR, Thermo Scientific, Waltham, MA, USA) fitted with an ATR cell. A thin layer of epoxy CAN sample was deposited on the ATR cell at room temperature. Spectra were taken for the samples. The spectrum of each sample is the averaged result from 32 scans collected from 550⁻¹ to 4000 cm⁻¹ at 1 cm⁻¹ resolution.

2.4. Viscosity measurement

At the early stage of re-polymerization, the solution viscosity was measured to identify the evolution of the average molecular weight of chain segments. After respectively heating at 160, 180, and 200° C for different times, the solution viscosity was measured by using a rheometer (TA Instruments, AR-G2, New Castle, DE, USA) with the parallel plate geometry (20-mm diameter, $1000-\mu$ m gap). During the measurements, the temperature was maintained constant at room temperature, and the shear rate was increased from 10^{-3} to 200 s^{-1} .

2.5. Volume shrinkage measurements

Volume-shrinkage induced residual stress has been a major concern during the fabrication of thermosets and their composites. When it comes to the solvent-assisted recycling of CANs, volume shrinkage of the resin during the re-polymerization could be noticeable due to the evaporation of solvent molecules. To characterize the volume changing of the re-polymerizing networks, the decomposed polymer solution was first heated at 200°C for re-polymerization. After 4 hours, the resin passed gelation and can carry the load. It was then cut into specimens and mounted on the Dynamic Mechanical Analysis (DMA, Model Q800, TA Instruments, New Castle, DE, USA) machine at constant temperatures (160, 180, and 200°C, respectively). No force was applied, and the sample was in the free-standing state. The volume change was recorded as a function of time. Note that thin-film epoxy samples with a thickness of 0.5 mm were tested, which exhibit a uniform solvent content and network properties in the thickness direction during the re-polymerization.

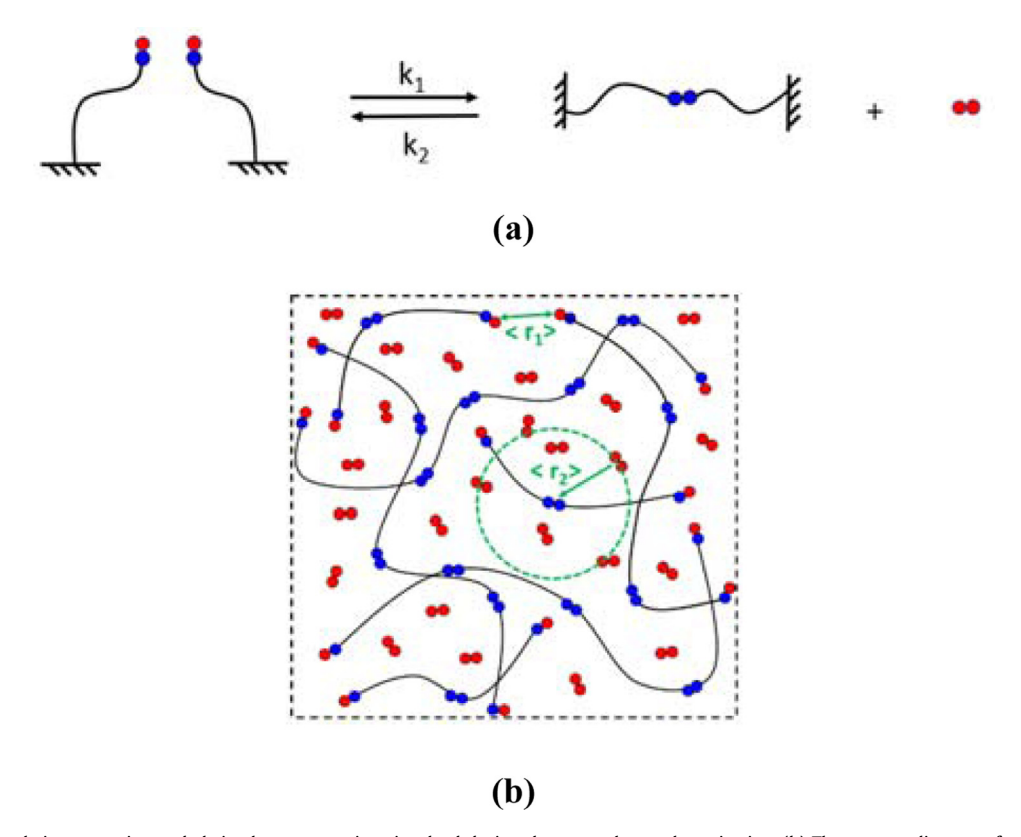


Fig. 4. (a) The chain connection and chain cleavage reactions involved during the network re-polymerization. (b) The average distance of reactive sites on the chain segment tail $\langle r_1 \rangle$, and the average distance between the solvent molecules and the segment tails $\langle r_2 \rangle$. The blue circles denote the ester bonds on the backbone of chain segments, and red circles denote the hydroxyl functional group. (For interpretation of the references to color in this figure legend, the reader is referred to the web version of this article.)

2.6. Dynamic mechanical analysis

DMA tests were conducted to measure the evolution of network modulus and glass transition behavior of thin-film epoxy samples during the re-polymerization (after gelation). During the DMA experiments, the samples with the same dimension of 12 mm \times 3 mm \times 0.5 mm were first stabilized at -30° C for 10 min to reach the thermal equilibrium. Then the strain oscillated at a frequency of 1 Hz, and the temperature was increased from -30 to 100° C at a rate of 2° C min $^{-1}$.

3. A multiscale constitutive model

3.1. The overall model description

The overarching modeling strategy is described as following: in the microscale, we formulate the rates of chain connection and cleavage during the re-polymerization based on the diffusivity of solvent molecules and chain segments as well as their contents and average distance. The rate constants are then used in first-order reaction equations to formulate the content and length distribution of chain segments during the CAN re-polymerization. A DoC parameter is defined based on the conversion of functional groups, which is used to capture the FTIR results and resin viscosity. The DoC parameter is used as an internal variable in a continuum-level multi-branched model to capture the volume shrinkage and evolution of network thermo-viscoelastic properties.

3.2. The microscale model: the kinetics of re-polymerization

The re-polymerization process of CANs involves chain connection and chain cleavage (Fig. 4(a)). The chain-connection reaction is that two short chain segments connect at the tail to form a longer segment and generate a solvent molecule. The reverse reaction leads to the chain cleavage. With the generated solvent molecules gradually evaporating out, the system equilibrium shifts to the re-polymerization, and the average chain segment length increases. The rates of chain connection and cleavage reactions (k_1 and k_2) are determined by the two time-dependent processes: the diffusion of reactive species and the transesterification reaction. The first process depends on the content and relative distance of reactive species

(Fig. 4(b)). For example, during the chain connection, two chain segments first diffuse towards each other and then connect. Therefore, the reaction rate depends on the average distance among the exchangeable bonds at the segment tails, $< r_1 >$. On the other hand, the chain cleavage rate depends on the distance between solvent molecules and ester groups on the chain backbone, $< r_2 >$.

3.2.1. Rate of chain connection k₁

During the chain connection reactions, since the reactive bonds are attached to the chain segments, their movement follows Rouse sub-diffusive motion, rather than the random Brownian diffusion. The mean-square traveling displacement increases as the four roots of time *t* (Degennes and Gennes 1979, Degennes 1982, Rubinstein and Colby 2003):

$$\langle R \rangle = b \left(\frac{t}{\tau_{0i}} \right)^{1/4},\tag{1}$$

where b is the monomer length, and τ_{0i} is the Rouse time of the chain segments with i monomers on the backbone. If the Rouse time of the shortest segment is τ_{0s} , the Rouse time of the segment with i monomers will be (Rubinstein and Colby 2003):

$$\tau_{0i} = i^2 \tau_{0s}. \tag{2}$$

On the other hand, the temperature dependency of Rouse time can be described using the time-temperature superposition principle (Williams et al. 1955, O'Connell and McKenna 1999, Rubinstein and Colby 2003):

$$\tau_i(T) = \tau_{0i}\alpha(T),\tag{3}$$

$$\log_{10}\alpha(T) = -\frac{c_1(T - T_g)}{c_2 + (T - T_g)},\tag{4}$$

where τ_i is the Rouse time at any temperature, τ_{0i} is the Rouse time at the glass transition temperature (T_g), T is the temperature, and c_1 , c_2 are empirical constants.

We denote C_i to be the volume concentration of chain segments with i monomers. Each segment has two exchangeable bonds at the tail, so, the concentration of exchangeable bonds at a continuum point is written as $C_r = 2\sum_{1}^{N-1} C_i$, where N is the amount of monomers in each polymer chain when the network is fully polymerized. The relative distance among exchangeable bonds is:

$$\langle r_1 \rangle \approx (C_r N_A)^{-1/3},\tag{5}$$

with N_A being the Avogadro's number (6.02 \times 10²³ mol⁻¹).

For a segment with i monomers, its traveling time (t_1) to meet another reactive site at segment tails can be obtained by solving:

$$b\left(\frac{t_1}{\tau_i}\right)^{1/4} = \langle r_1 \rangle,\tag{6}$$

which gives:

$$t_1 = \frac{\tau_i}{(C_r N_a b^3)^{4/3}},\tag{7}$$

Following the previous works (Yu et al. 2017), the average time spent on a BER is related to the BER energy barrier, E_{ab} , as $t_{BER} = t_{0_BER} \exp(E_{ab}/RT)$, with t_{0_BER} being a time constant. R=8.31 J mol⁻¹ K⁻¹ is the gas constant. Overall, the reaction rate (mol/s) for the chain connection can be written as:

$$k_1 = (N_A t_1 + N_A t_{BFR})^{-1}$$
. (8)

3.2.2. Rate of chain cleavage k2

During the chain cleavage reaction, we assume that there are n solvent molecules in average around each ester group. For the chain segment with i monomers, there are i-1 ester groups on the chain backbone. If the concentration of solvent molecules at a material point is denoted as C_0 , we have:

$$n = \frac{C_0}{\sum_{i=2} (i-1)C_i}. (9)$$

The average distance between an ester and solvent molecule is formulated by the theory of mean inter-particle distance, which was first derived by Chandrasekhar (1943) based on the probability distribution function of distance to the nearest neighbor particle:

$$\langle r_2 \rangle = \frac{1}{3} \Gamma\left(\frac{1}{3}\right) a,\tag{10}$$

where Γ is the gamma function, and a is the Wigner–Seitz radius which is defined by:

$$a = 3\sqrt{\frac{4N_A\pi C_0}{3}}. ag{11}$$

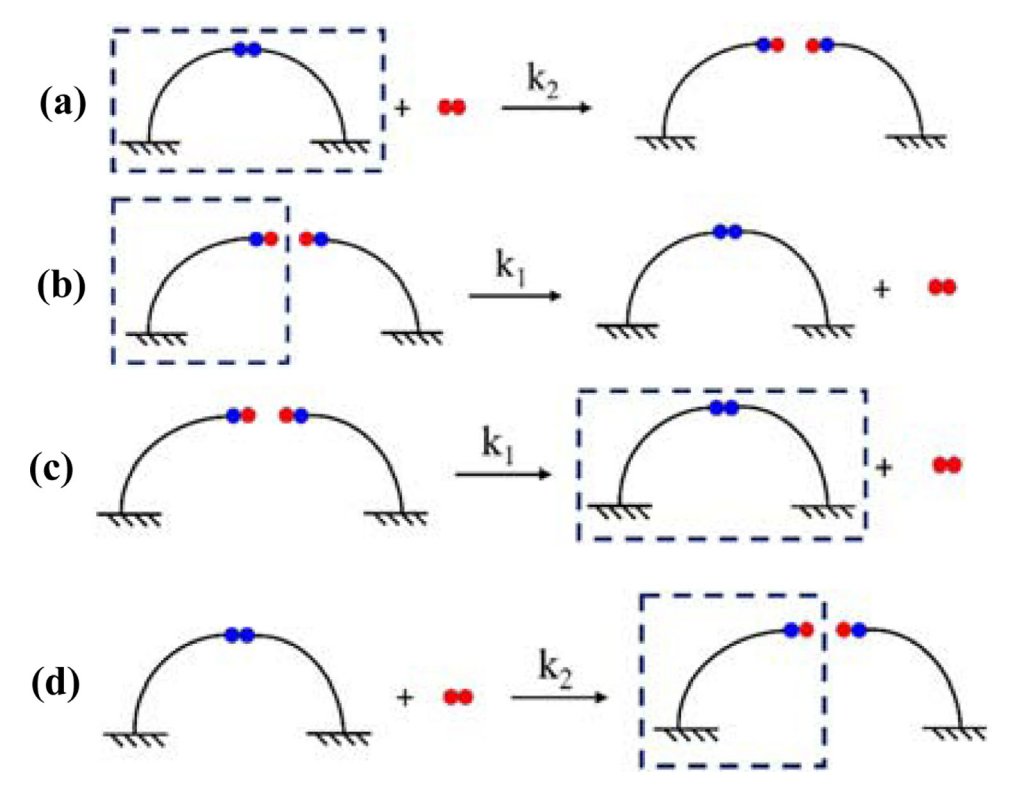


Fig. 5. Four types of exchange reactions that can change the segment length. The segment with i monomers is highlighted with dash box. The blue circles denote the exchangeable bonds on the backbone of chain segments and red circles denote the EG solvent molecule. (For interpretation of the references to color in this figure legend, the reader is referred to the web version of this article.)

Since the solvent molecules are not linked to the chain segment, we assume their movement during the chain cleavage reaction follows the Brownian-like motion. According to Albert Einstein's Theory of Brownian Motion (Einstein 1905), the mean-squared displacement during the random walk of solvent molecules is in a linear relationship with the traveling time. Therefore.

$$t_2 = \frac{\langle r_2 \rangle^2}{D_s},\tag{12}$$

Note that D_s is the diffusivity of solvent molecules, which was shown by to be the self-diffusion of solvent within the polymer networks (Rudin and Choi 2013), and thus can be measured using polymer swelling tests.

The reaction rate for the chain cleavage (mol/s) can be determined by:

$$k_2 = (N_A t_2 + N_A t_{BFR})^{-1}$$
 (13)

3.2.3. Statistical analysis of segment length distribution

Statistical analysis is performed to determine the content and length distribution of the chain segments. During the network synthesis, ester groups on the chain backbone were formed by the epoxy-carboxyl reaction. Since the stoichiometric ratio between the fatty acid and epoxy is 1:1, we can safely assume that the ester bonds are evenly distributed on the backbone of chain segments, and their spacing equals the average length of constituent monomers.

During the re-polymerization, there are four types of BERs that will change the content of the segment with i monomers (i.e. C_i). As illustrated in Fig. 5, the four reactions are: (a) a segment with i monomers reacts with a EG molecule and breaks into two shorter segments; (b) a segment with i monomers reacts with another chain segment to form a longer chain segment and generate a new EG molecule; (c) two short chain segments react to form a segment with i monomers and generate a new EG molecule; (d) a long chain segment react with an EG to form a segment with i monomers and another chain segment.

At a given material point, we assume that if the reactive species (chain segments and solvent molecules) exist during the network re-polymerization, their content is sufficient, so the four possible reactions shown in Fig. 5 are parallel reactions. Therefore, the changing rate of C_i is the summation of the reaction rates of the four reactions illustrated in Fig. 5:

$$\dot{C}_i = r_i^a(t) + r_i^b(t) + r_i^c(t) + r_i^d(t). \tag{14}$$

It should be noted that the four types of BER are not equally possible. Their magnitudes depend on the contents of reactant segments. Previous works have revealed that transesterification is a first-order reaction (Saroso 2016). The r_i^a is expressed as:

$$r_i^a = -k_2 C_i. ag{15a}$$

A negative sign is given in Eq. (15a) because each reaction (a) consumes a segment with i monomers. Similarly, the rate of reaction (b), r_i^b , is written as:

$$r_i^b = -k_1 C_i. \tag{15b}$$

For the reaction (c), a chain segment with j (j < i) monomers connects with another segment with (i– j) monomers. The reaction rate, r_i^c , is expressed as:

$$r_i^c = k_1 \sum_{i=1}^{i-1} C_j p_c,$$
 (15c)

where $p_C = C_{i-j}/\sum_m C_m$ is the probability to find a segment with (i-j) monomers at a material point.

For the reaction (d), a chain segment with j (j > i) monomers cleavages into two short segments. r_i^d is expressed as:

$$r_i^d = k_2 \sum_{j=i+1} C_j p_d, \tag{15d}$$

where p_d is the probability that one of the two generated short segment has i monomers. For the segment with j (j > i) monomers, there are (j-1) ester groups on the backbone. A segment with i monomers can be generated by breaking two specific ester groups. Therefore, $p_d = 2/(j-1)$.

Solving these linear differential equations will obtain the mole density (C_i) of chain segments with i monomers. The average monomer number of chain segments

$$\overline{N}(t) = \sum_{i=1}^{\infty} iw(t), \tag{16}$$

with

$$w_i = \frac{C_i}{\sum_{k=1} C_k}.\tag{17}$$

The reaction rates of four possible reactions in Fig. 5 also determine the changing rate of solvent content (C_0) at a material point:

$$\dot{C}_0 = \sum_{i=1} \left(r_i^a - r_i^b + r_i^c - r_i^d \right) - r_0, \tag{18}$$

In the above equation, r_0 is the consumption rate due to the solvent evaporation on the polymer-air interface. On the one hand, the solvent evaporation reduces the amount of solvent molecules in the mixture, and thus tends to reduce their volumetric content. On the other hand, the mixture thickness decreases, which tends to increase the solvent content. Following the previous works by Es-haghi and Cakmak (2015) and Xu and Liu (2019), the expression of r_0 is derived to be:

$$r_0 = -\frac{J_e}{w} + C_0 \frac{J_e M_c}{\rho w}. ag{19}$$

In the above equation, J_e (mol/m²s) is the solvent evaporation flux on the polymer-air interface, which follows $J_e = K_c C_0$, with K_c (m/s) being the average mass transfer coefficient. ρ is the solvent density, M_c is the molecular weight of the solvent the mixture thickness, W(t) is the mixture thickness. The detailed derivation process can be found in the supplementary material (Section S1).

3.3. Degree of curing: the linkage between the network microstructure and macroscopic material properties

During the polymerization, chain segments connect to form longer chains. To capture the evolution of material properties, it is straightforward to first describe the number distribution of polymer chains with different lengths, and then calculate the material properties by the superposition method. However, this could quickly become a daunting job due to the complex distributions of the chain segment length. To solve the problem, an alternative approach is to define a proper characterization parameter that links the microscale network structure to the continuum-level material properties. The degree of curing (DoC, varies from 0 to 100%) that formulates the conversion rate of monomers or functional groups is a good indication of the averaged composition of the system. It can be linked to many material properties and is easier to measure than the distribution of polymer chains. For example, the DoC can be measured through reaction entropy by differential scanning calorimetry (DSC), infrared spectroscopy absorbance by Fourier transform infrared spectroscopy (FTIR) and NMR spectrum. Because of these, the DoC is often used as the internal variable to characterize and model the property changes during the curing of thermosetting epoxy and adhesives (Gan et al. 1991; Watts and Silikas 2005; Dewaele et al. 2006).

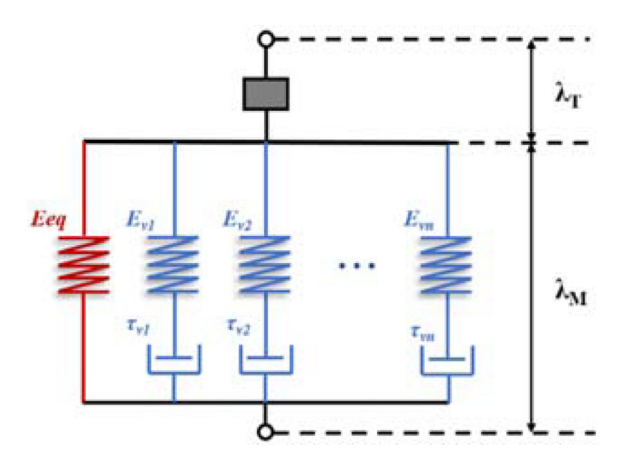


Fig. 6. The one-dimensional rheological model for the viscoelastic mechanical properties modeling. Red and blue parts of these branches respectively describe the equilibrium branches and viscoelastic branches. (For interpretation of the references to color in this figure legend, the reader is referred to the web version of this article.)

During the re-polymerization of epoxy vitrimer, each chain connection reaction generates an ester group on the chain backbone, and its content is a suitable parameter to define the DoC. At the beginning of re-polymerization, the system contains the shortest segments with content of $C_I(t=0)$. When the network is fully polymerized, the chain density can be written as $C_I(t=0)/N$, with N being the amount of monomers in each chain. Since each polymer chain contains (N-1) ester group on the backbone, the content of the backbone ester group in the fully cured epoxy can be written as $C_I(t=0)$ (N-1)/N. During the re-polymerization, the system has a distribution of polymer chains with different segment length. The DoC is defined to be the amount of ester groups on the segment backbone, $\sum_{i=2} (i-1)C_i(t)$, normalized by its final value in the fully polymerized network:

$$P(t) = \frac{N\sum_{i=2} (i-1)C_i(t)}{(N-1)C_1(t=0)}.$$
 (20)

3.4. The continuum-level model

3.4.1. Overview of the multi-branched model

The thermomechanical behaviors of polymers have been intensively studied in recent decades. There are mainly two streams for the theoretical modeling efforts. The first one is based on the rheological models using linear rheology elements (spring elements and dashpot elements), which are consistent with the inherent viscoelasticity of amorphous polymers (Nguyen et al. 2010, Srivastava et al. 2010, Diani et al. 2012, Yu et al. 2016, Gu et al. 2017). For example, the temperature-dependent relaxation times of dashpots are corresponding to the mobility change of polymer chains in the amorphous polymers. It should be noted that such a model usually contains many parameters that need to be calibrated from experiments. To this end, the phase-evolution models (Chen and Lagoudas 2008, Qi et al. 2008, Kim et al. 2010, Yang and Li 2016, Li and Liu 2018, Pan et al. 2018) based on the evolution between hard and soft phases is more concise to use, specifically for the study of semi-crystalline polymers with phase evolution mechanisms.

In this work, the viscoelastic properties of amorphous CANs are studied using a multi-branched rheological models, which was successfully applied in our previous works to study the amorphous polymers (Yu et al. 2012, 2014). The DoC is used as an internal variable in the continuum-level multi-branch model to study the thermo-viscoelastic behaviors of re-polymerizing CANs. Fig. 6 shows the rheological analogy of this model. A thermal expansion element is arranged in series with mechanical elements. The mechanical elements consist of two parts: the equilibrium branch represented by an elastic spring and the non-equilibrium Maxwell branches that describe the relaxation of viscoelastic polymer chains. It should be noted that the continuum-level model captures the network properties of thin-film material with uniform solvent concentration. The re-polymerization of thick samples that involves diffusion of solvent molecules in the sample thickness direction will be studied in the future.

The total deformation of CAN network is decomposed into thermal and mechanical parts:

$$\lambda = \lambda_M \lambda_T, \tag{21}$$

where λ is the total stretch ratio of the model. λ_M and λ_T are the stretching ratios of the thermal and mechanical components, respectively. Following the previous work (Dewaele et al. 2006), a linear relationship between the volume shrinkage and the DoC is assumed $\Lambda = (V_0 - V)/(V_0) = \chi P$, with χ being a fitting parameter. The stretch ratio of the thermal component is written as:

$$\lambda_T = 3\sqrt{1 - \chi P}.\tag{22}$$

The true stress σ of the model is the summation of each paralleled components

$$\sigma = \sigma_{eq} + \sum_{i=1}^{n} \sigma_{\nu j},\tag{23}$$

where σ_{eq} and σ_{vj} , are respectively, the true stresses of the equilibrium branch and viscoelastic branches. Each branch has the same stretch, λ_M .

To calculate the true stress of the equilibrium branch, we adopt the following simple large-deformation elasticity model:

$$\sigma_{eq} = E_{eq}(t) \ln[\lambda_M(t)], \tag{24}$$

where the network equilibrium modulus, E_{eq} , evolves during the re-polymerization. The detailed evolution rule is given in the next section. The logarithm of strength ratio defines the true strain, which conveniently converts the multiplicative operation of stretches into additive strains, which greatly simplifies the numerical iterations. Note that the same relationship was used in the previous works (Westbrook et al. 2010, Ge et al. 2013, Hanzon et al. 2019) to calculate the true stress of soft materials. For viscoelastic branches, the stress can be calculated by:

$$\sigma_{\nu j} = E_{\nu j} \ln(\lambda_{\nu j}^e) = E_{\nu j} \tau_{\nu j} \frac{1}{\lambda_{\nu j}^{\nu}} \frac{d\lambda_{\nu j}^{\nu}}{dt}, \tag{25}$$

where E_{vj} and λ^e_{vj} are respectively, the elastic modulus and stretch ratio of the spring. τ_{vj} and λ^v_{vj} are respectively, the relaxation time and stretch ratio of the dashpot in the jth viscoelastic branch. λ^v_{vj} and λ^e_{vj} can be related to the stretch ratio of mechanical component as: $\lambda_M = \lambda^v_{vj} + \lambda^e_{vj} - 1$.

3.4.2. The evolution of equilibrium modulus

Following the previous work (Daoud 2000), the equilibrium modulus is scaled with the correlation length of chain segments, l_0 , by:

$$E_{eq} = \frac{k_b T}{l_0^3},\tag{26}$$

where k_b is Boltzmann constant (1.38 \times 10⁻²³ m² kg s⁻² K⁻¹). l_0 is further scaled with the DoC by (Adolf et al. 1990, Rubinstein and Colby 2003):

$$l_0 \sim P^{-2\beta_v}$$
, (27)

where β_V is a correlation exponent. Combining Eqs. (25) and (26), the evolution of network equilibrium modulus during the re-polymerization is written as:

$$E_{eq} = E_{\infty} P^{6\beta_v}. \tag{28}$$

where E_{∞} is the equilibrium modulus of a fully cured network.

3.4.3. Evolution of relaxation time

The relaxation time of each Maxwell element is a function of temperature. Based on the time-temperature superposition principle (TTSP), τ_{vi} can be written as (Rubinstein and Colby 2003):

$$\tau_{vi}(T) = \tau_{vi0}\alpha_v(T). \tag{29}$$

In the above equation, τ_{vj0} is the relaxation time at the network glass transition temperature (T_g) . $\alpha_v(T)$ is the shift factor which can be respectively described by the Williams–Landel–Ferry equation above T_g and by the Arrhenius equation below T_g . (Williams et al. 1955, Di Marzio and Yang 1997)

$$\ln\left[\alpha_{\nu}(T)\right] = \frac{AF_{c}}{k_{b}} \left(\frac{1}{T + 273.15} - \frac{1}{T_{g} + 273.15}\right) \text{atT} < T_{g},\tag{30a}$$

$$\log \left[\alpha_{\nu}(T)\right] = -\frac{c_1(T - T_g)}{c_2 + T - T_g} atT > T_g.$$
(30b)

Here, A and F_c material specific constants. c_1 and c_2 are fitting parameters that are the same as used in Eq. (4).

In Eq. (29), the shift factor decreases with the temperature, which is corresponding to the increment of chain mobility and fast viscoelastic relaxation. On the other hand, because the newly formed network will hinder the old networks from relaxing, the shift factor in Eq. (29) increases with the network T_g , which suggests a gradually increased network relaxation time.

3.4.4. The evolution of network Tg

The glass transition temperature is an important indication of the extent of curing. The relationship between the T_g and the DoC has been widely studied before. Gan et al. (1991) developed a viscoelastic type model for the curing polymer by using the empirical Dibenedetto equation (Nielsen 1969, DiBenedetto 1987). The model considers the mobility of polymer chains in the curing network and can well capture the T_g evolution of various polymer systems. Following this work, the T_g of CANs during the re-polymerization is written as:

$$T_{g} = \frac{E_{r}}{R \ln \left[g_{1} (1 - P)^{\xi} + g_{2} \right]},$$
(31)

where $E_{\rm r}$ is the activation energy of transition from the glassy to the rubbery state, ξ is the parameter for accounting the effects of chain entanglement. g_1 , g_2 are two material constants.

4. Results and discussions

4.1. Material parameters identifications

During the network decomposition, the mole number of EG solvent molecules was the same as the ester group on the chain backbone. In this manner, the fully decomposed network contains only the shortest chain segment, and there are negligible unreacted solvent molecules in the system. The initial volume content of the shortest chain segment $C_I(t=0)$ can be determined by the ratio of DGEBA and fatty acid during the network synthesis. For the precursor chemicals, DGEBA and fatty acid have a molecular weight of 340 and 601.9 g/mol, respectively, and their stoichiometry ratio was 1:1. Assuming the density of the polymer solution is 1g cm⁻¹, $C_I(t=0)$ is calculated to be 7.8 × 10⁵ mol/m³. The volume contents of other chain segments C_i (i>=2) are set to be 0.

When the network is fully polymerized, the chain length follows a specific distribution. However, using existing polymer characterization techniques, it remains challenging to determine the detailed chain length distribution in the crosslinked networks. Therefore, in this paper, for the convenience of analysis, we assume the uniform length of polymer chains. With this assumption, the numerical predictions in the later sections are shown to be close to the experimental data. The detailed influences of chain segment length deserve our further study. Following the previous works on the same material, we set the average length of monomer, *b*, to be 1 nm, and the amount of monomers on the chain backbone in the fully polymerized network (*N* in Eq. 20) to be 8 (Long et al. 2013, Yu et al. 2016, Yu et al. 2017).

4.1.1. Evaporation rate of EG solvent

The changing rate of C_0 due to the solvent evaporation (r_0 in Eq. (19)) is a major parameter to determine the repolymerization rate. To determine the mass transfer coefficient K_c (m/s), a mixture of polymer solution was prepared containing monomer DGEBA and cross-linker fatty acid. Their stoichiometry ratio was identical to that in the synthesized epoxy CANs. 30 wt% EG (compared to the mixture mass) was added. Based on the solvent and monomer density, the initial solvent volume fraction was estimated to be 4.52×10^3 mol/m³ The mixture was poured into a model with ~1.8mm thickness and ~900mm² evaporation area. The mixture was then heated at 120° C, 140° C, 160° C, and 200° C respectively to measure the mass loss. No phase evolution was observed within the mixture at high temperatures. Note that due to the excessive solvent and no BER catalyst, there was no chemical reaction involved during the heating, and the mixture mass drop mainly resulted from the solvent evaporation.

Fig. S1 shows the drop of mass as a function of heating time and temperature. The solvent mass can be predicted by Eq. (19). By fitting with the experimental data, the mass transfer coefficient, K_c , at these three temperatures are determined to be 4.8×10^{-8} , 1.3×10^{-7} , 4.8×10^{-7} , 9.6×10^{-7} , 2.2×10^{-6} m/s, respectively. The detailed procedure and experimental results are summarized in the supplementary material (Section S1). To assist the parametric studies in this paper, an exponential equation is proposed to describe the relationship between the evaporation rate K_c and temperature T:

$$K_c(T) = a_1 \exp(-a_2/RT).$$
 (32)

where R is the gas constant. As shown in Fig. S2, when the fitting parameters a_1 and a_2 are set to be 8×10^4 m/s and 9.5×10^4 J/mol, respectively, the proposed equation closely captures the values of K_c at different temperatures.

4.1.2. The diffusivity of EG within the network

The diffusivity of EG in the epoxy network, D_s , determines the rate of chain cleavage (Eq. (12)) and is measured by the swelling tests. Epoxy samples without the BER catalyst were soaked in the EG solvent at different temperatures. Without the catalyst, the samples behaved like conventional thermosets and kept swelling without decomposition. At times, their weight was measured to determine the solvent diffusivity. The detailed experimental procedure is described in the supplementary material (Section S2). The temperature dependence of D_s follows the Arrhenius equation:

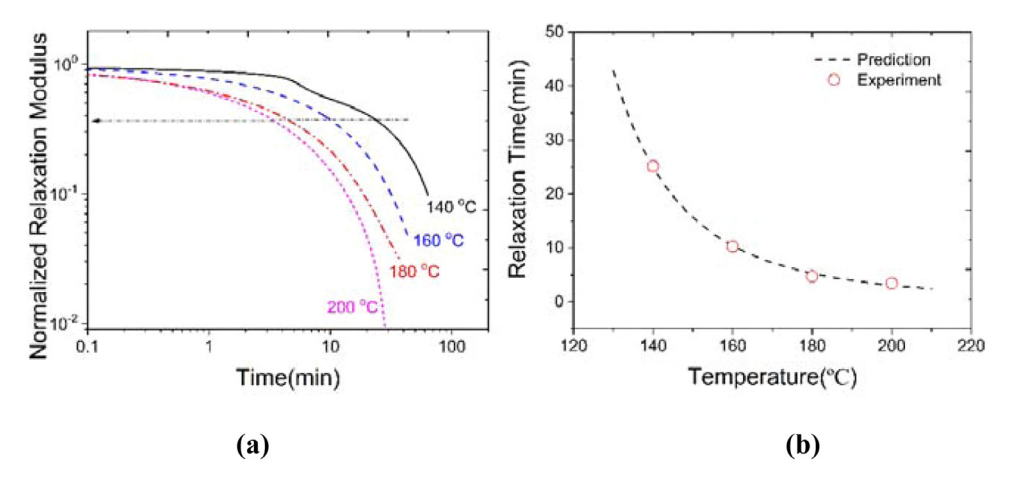


Fig. 7. (a) Stress relaxation behavior of fresh epoxy CAN. The relaxation time is determined to be the time point when the relaxation modulus reduces by 63.2% (the dash line) (b) the relationship between relaxation time and temperature.

$$D_s(T) = D_{s0} \exp\left(-\frac{E_{as}}{RT}\right),\tag{33}$$

where D_{s0} is the reference diffusivity, E_{as} is the activation energy. In Fig. S3, by fitting the experimental data, the corresponding parameters were determined to be $E_{as} = 34.2$ kJ/mol and $D_{s0} = 3.23 \times 10^{-6}$ m²/s.

4.1.3. BER kinetics and activation energy

The BER energy barrier, E_{ab} , determines the average time spent on a BER and the chain connection and cleavage rates (as shown in Eqs. (8) and (13)). E_{ab} was measured by performing a series of stress relaxation tests on the as-fabricated epoxy CAN at different temperatures (Yu et al. 2014). During the stress relaxation tests, the normalized relaxation modulus (Fig. 7(a)) was used to identify the relaxation time τ_{BER} , which is taken to be the time point when the normalized relaxation modulus declines to 1/e (~36.8%). The relaxation times are summarized in Fig. 7(b) as a function of temperature.

Previous studies show that τ_{BER} can be written as:

$$\tau_{BER} = k_0 \exp\left[\frac{E_{ab}}{RT}\right],\tag{34}$$

where the k_0 is a correlation exponent. By fitting the experimental data in Fig. 7(b), BER energy barrier is determined to be E_{ab} =8.15 kJ/mol.

4.1.4. Parameters for the multi-branched model

The material parameter of volume shrinkage χ (in Eq. (22)) was determined by fitting with the tested volume change of epoxy vitrimer during the re-polymerization at 180°C. The glass transition behavior of epoxy vitrimer was measured at different stages of re-polymerization. The tested rubbery moduli were used to determine the parameters of equilibrium branch (E_{∞} and β_{ν} in Eq. (28)), and the tested T_{g} was used to identify the parameters in Eq. (31). The detailed curve-fitting results are shown in the supplementary material (Sections S3–S5).

Parameters for the viscoelastic branches (elastic moduli E_{vj} , relaxation times τ_{bi} , and TTSP parameters) were determined by performing a group of stress relaxation tests on the as-fabricated epoxy CANs around its network T_g . The relaxation curves are plotted in Fig. 8(a). Based on the time-temperature superposition principle (TTSP), each curve is shifted to the T_g (27°C) to form a master relaxation curve Fig. 8(b)). The corresponding shifting factors are plotted in Fig. 8(c) as a function of temperature. At temperatures above and below T_g , the shift factors are respectively captured by the WLF and Arrhenius equations (Eq. ((30))). The corresponding parameters were determined to be AF_c/k_b =-40070, c_1 =3.8, and c_2 =18.5 °C.

After obtaining the master relaxation curve, it is used to determine the modulus and relaxation times of each branch using the nonlinear regression method. (Sherrod 2000, Diani et al. 2012). As shown in Fig. 9, when adding 11 nonequilibrium branches, the model prediction curve rejoins with the experimental master curve. The corresponding E_{bi} and τ_{bi} values are listed in Table 1.

4.2. Conversion of the hydroxyl group during re-polymerization

The developed chemomechanics theory can be used to capture the network microstructure during the re-polymerization, which is characterized by the conversion ratio of functional groups. In Fig. 10(a), the content of the hydroxyl group within the system is represented by the absorbance peaks of the FTIR curves. It is observed that the hydroxyl content gradually decreases as re-polymerization proceeds because the newly formed EG molecules evaporate out of the system. After being

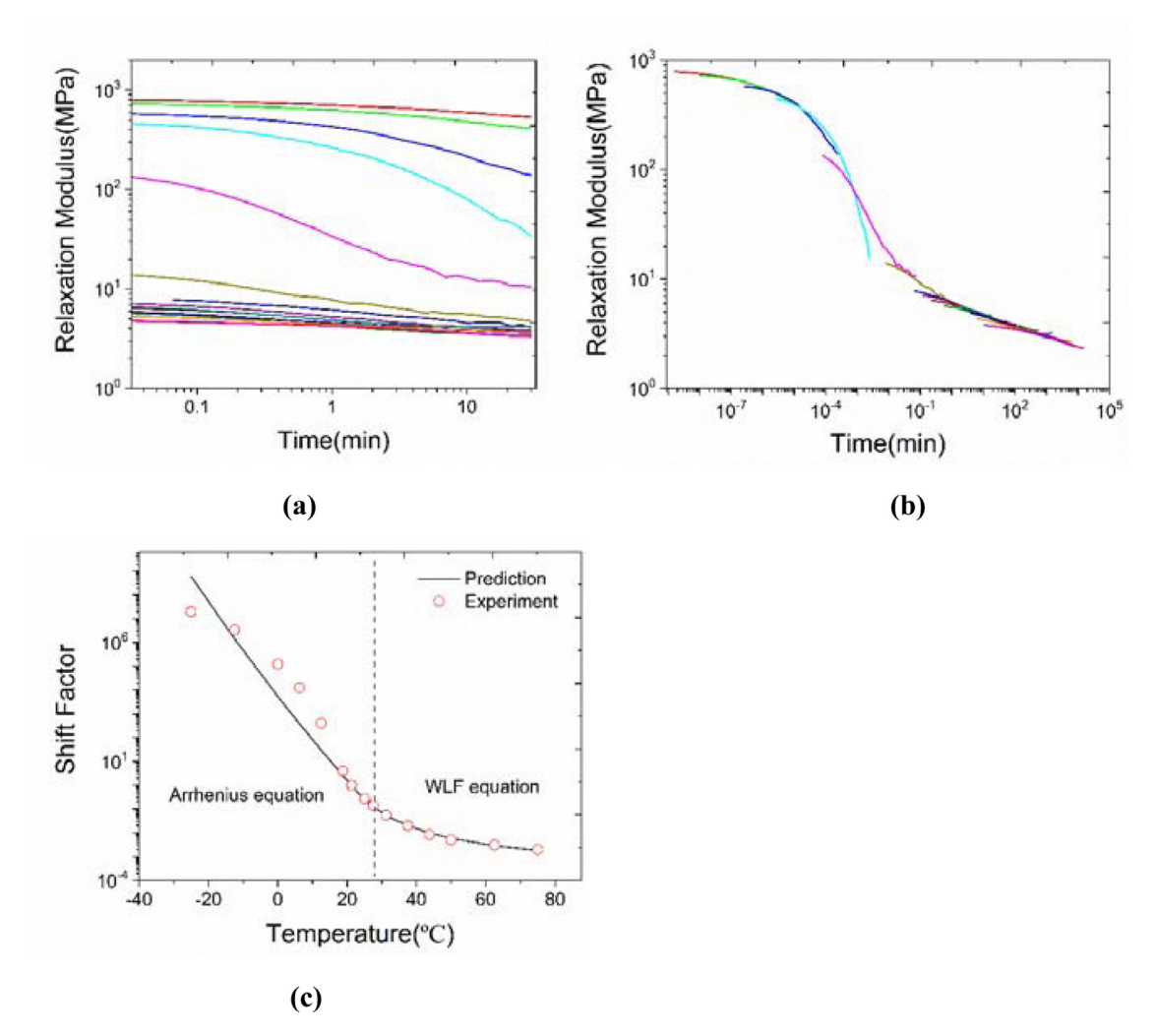


Fig. 8. (a) The relaxation moduli of viscoelastic branches; (b) Master curve after shifting each temperature to T_g (17°C). (c) Shift factor in each temperature. Red circles are the experimental data, and the black solid line is the predictions of Arrhenius and WLF equation. (For interpretation of the references to color in this figure legend, the reader is referred to the web version of this article.)

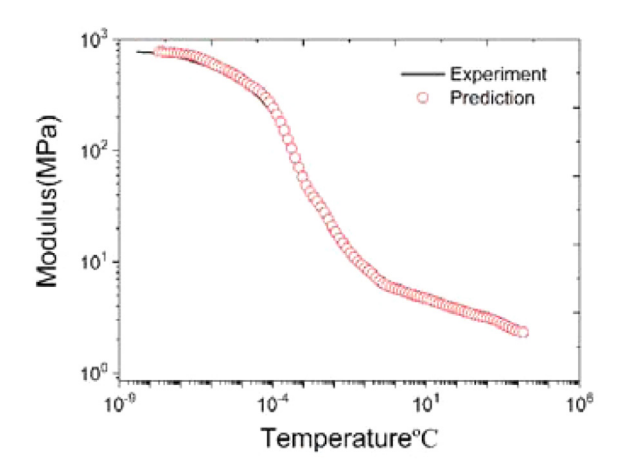


Fig. 9. Master curve fitting with 11 viscoelastic branches added into the model. Red circle line is model prediction, and the black solid line is the experimental master curve. (For interpretation of the references to color in this figure legend, the reader is referred to the web version of this article.)

Table 1Parameters in the multi-scale chemomechanics model.

Description	Symbol	Value
Parameters of the microscale model		
Fitting parameter for K_c	a_1	$8 \times 10^4 \text{ m/s}$
Fitting parameter for K_c	a_2	9.5×10^4 J/mol
Energy barrier for solvent diffusion	E_{as}	34.2kJ/mol
Reference diffusivity	D_0	$3.23 \times 10^{-6} \text{m}^2/\text{s}$
Energy barrier for BER	E_{ab}	8.15 kJ/mol
Monomer length	b	1 nm
The largest monomer number in the polymer chains	N	8
Rouse time of the shortest segment at T_g	$ au_{0s}$	0.1s
Parameters of the continuum-level model		
Parameter for volume shrinkage	χ	0.435
Activation energy of glass transition	Χ E _r ξ	23.6 kJ/mol
Parameter for T_g	ξ	0.7
Parameter for T_g	g_1	21,100
Fitting parameter for T_g	g_2	11320
Equilibrium modulus of a fully cured network	E_{∞}	3.21 MPa
Parameter for equilibrium modulus	β_{ν}	1.3
Elastic moduli in each branch	E_{vi}	206, 240, 155, 80, 28, 18, 5, 0.6, 0.2, 0.501, 0.069 MPa
Relaxation times at T_g in each branch	$ au_{ u j}$	1×10^{-7} , 1×10^{-6} , 1.5×10^{-5} , 6×10^{-5} , 6×10^{-4} , 3×10^{-3} , 2.5×10^{-2} , 2.5×10^{-1} , 2.5 , 25 , 600 s
Parameter of WLF equation	c_1	3.8
Parameter of WLF equation	c_2	18.5°C
Parameter of Arrhenius equation	AF_c/k_b	40070

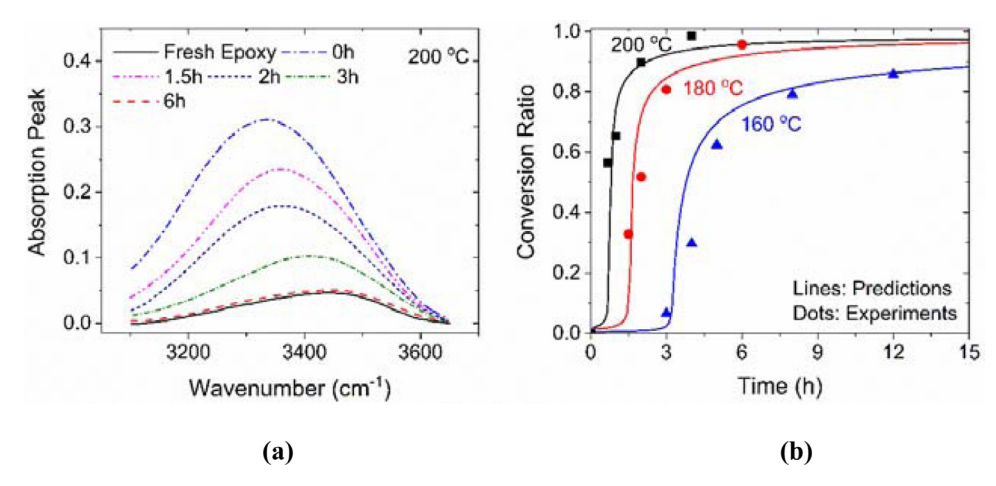


Fig. 10. (a) FTIR traces to monitor the content of -OH groups during epoxy re-polymerization. (b) Prediction on the conversion ratio of -OH group at different re-polymerization temperatures.

heated at 200°C for 6 h, the hydroxyl content reaches the same level as that of the fresh sample, which suggests the network microstructure is restored after recycling.

A close examination of the four possible BERs in Fig. 5 tells that the decreasing rate of EG molecules in the system is the same as the forming rate of ester groups on the chain backbone. Therefore, the content of the hydroxyl group is in a linear relationship with the DoC defined in Eq. (20):

$$P = \frac{h_0 - h(t)}{h_0 - h_\infty},\tag{35}$$

where h_0 is the absorbance peak of decomposed polymer solution at the beginning of re-polymerization, and h_∞ is the absorbance peak of the fully polymerized network. The experimental data and model predictions of DoC at different repolymerization temperatures are compared in Fig. 10(b). It is seen that the predictions agree well with the experimental results, where the conversion of the hydroxyl group first increases almost linearly with heating time and then slows down as it approaching 100%. The ever-decreasing conversion rate is due to increased distance among reactive sites at the tail of chain segments as the reaction proceeds.

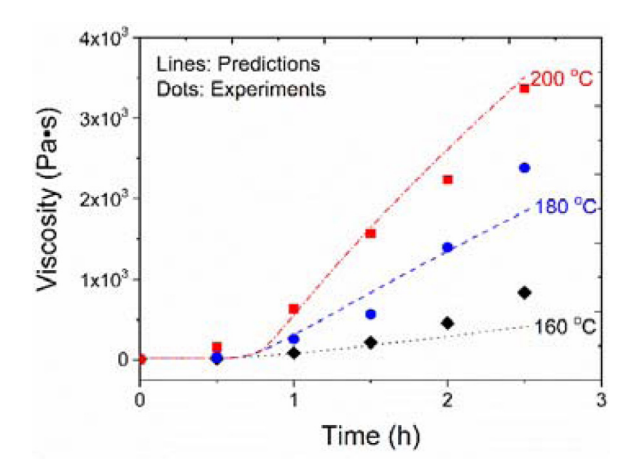


Fig. 11. Predictions of the viscosity during the CAN re-polymerization before gelation at 160°C 180°C and 200°C, respectively. Dots: experimental data. Dashed lines: Predictions.

4.3. Evolution of the viscosity during re-polymerization

The measured solution viscosities at different heating temperatures (160°C, 180°C, 200°C) are plotted as dots in Fig 11 as a function of time. During the re-polymerization, the short chain segments in the solution are connected by BERs. Therefore, the average molecular weight and the solution viscosity are gradually increased. The increment rate is higher at higher temperature due to the promoted rate of BERs and solvent evaporation.

Previous work (Rubinstein and Colby 2003) suggested that the viscosity of polymer solution, η , is scaled to the average molecular weight \bar{M} by:

$$\eta = k_p \bar{M}^{\alpha},\tag{36}$$

where α is 3.4 which is the empirical constant, and k_{η} is a fitting parameter. The developed chemomechanics theory predicts the content and length distribution of chain segments, which can be used to calculate the average molecular weight as: $\bar{M} = \sum_{i=1}^{N} i C_i M_1 / \sum_{i=1}^{N} C_i$. M_1 is the molecular weight of monomers, which is taken to be the average molar mass of DGEBA and fatty acid (233 g/mol). As shown in Fig. 11, the model predictions agree well with the experimental data when k_{η} is 1×10^{-5} mol/m/s.

4.4. Network volume shrinkage during the re-polymerization

During the re-polymerization of CANs, the Van-der-Waals interactions among chain segments converse into the covalent bonding. Solvent molecules are generated and evaporated out of the system. Both two mechanisms lead to the volume contraction of the resin. With a confined boundary condition, residual stress could be developed, which has been a major concern during the manufacturing of thermosets and their composites. It is therefore important to reveal the relationship between volume shrinkage and re-polymerization degree, which provide a guideline to design material and processing conditions for homogeneous network structure and mechanical properties of recycled thermosets. The decomposed polymer solution was initially heated at 200°C. After 4 hours, the samples passed gelation and were transferred to the DMA machine to measure the volume shrinkage at 160, 180, and 200°C, respectively. The experimental data is shown in Fig. 12. The rate of volume shrinkage is observed to increase with temperature. At 200°C, the sample volume is decreased by ~8% as the re-polymerization completes at ~6 hours. The data is also compared with the model predictions (dashed lines), in which the conversion ratio during the free-standing heating was first predicted, and then the volume shrinkage was calculated using Eq. (22). The good agreement between model predictions and experiments suggests that for a re-polymerizing CAN with solvent evaporation, the degree of volume shrinkage is still in a linear relation with the DoC.

4.5. Glass transition behaviors during the re-polymerization

The multiscale chemomechanics model was used to predict the glass transition behaviors of thermosets at different stages of re-polymerization. For the continuum-level multi-branched model, the temperature-dependent storage modulus E_s , loss modulus E_l , and tan?? are respectively expressed as:

$$E_s = E_{eq} + \sum_{i=1}^{N_b} \frac{E_{vj}\omega^2 \tau_{vj}^2}{1 + \omega^2 \tau_{vj}^2},$$
(37a)

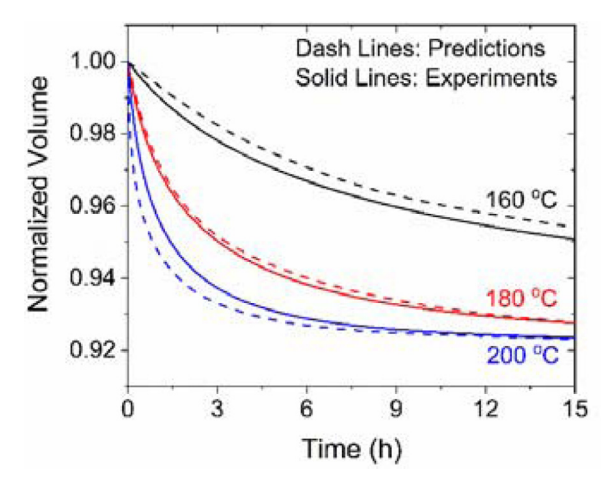


Fig. 12. Predictions of the network volume change during the re-polymerization at 160°C 180°C, and 200°C respectively.

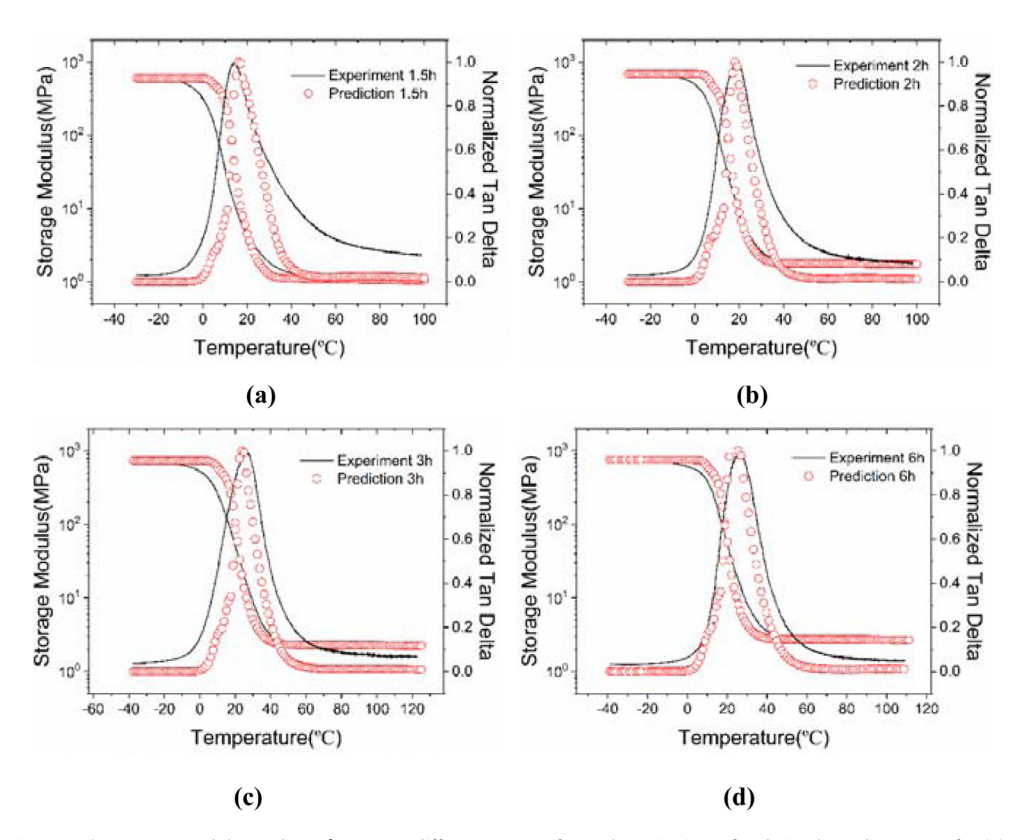


Fig. 13. Predictions on the storage modulus and $\tan \delta$ curve at different stages of re-polymerization, after being heated at 200°C for (a) 1.5h, (b) 2h, (c) 3h, and (d) 6h, respectively.

$$E_{l} = \sum_{j=1}^{N_{b}} \frac{E_{\nu j} \omega \tau_{\nu j}}{1 + \omega^{2} \tau_{\nu j}^{2}},$$

$$\tan \delta = \frac{E_{l}}{E_{s}},$$
(37b)

$$\tan \delta = \frac{E_l}{E_s},\tag{37c}$$

where ω is the testing frequency (1 Hz in the experiments).

The glass transition behavior of CAN at different stages of re-polymerization at 200°C was tested on the DMA machine, and the experimental results are compared with model predictions in Fig. 13. It can be seen that the predictions on the storage modulus and normalized tan δ agree well with the experimental data ranging from -20 to 80° C. The network

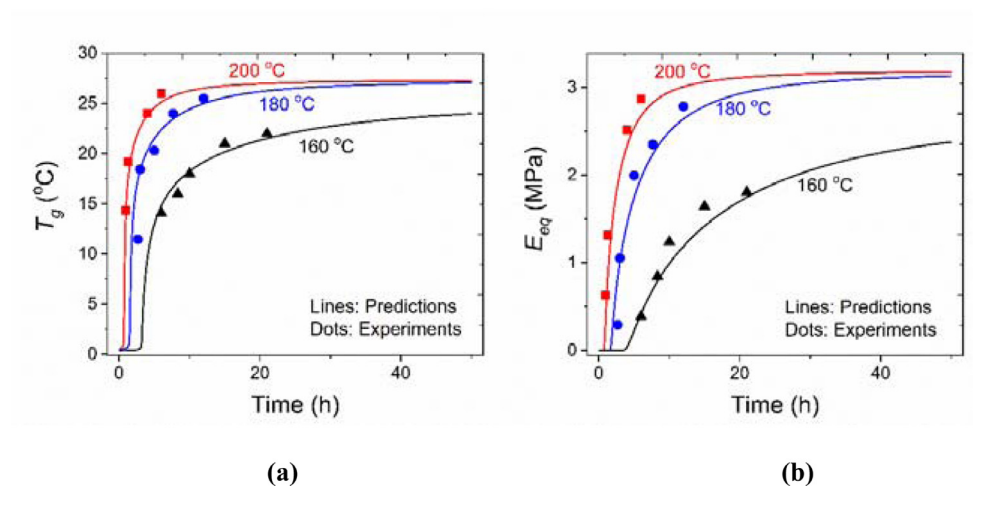


Fig. 14. Predictions on the evolution of (a) T_g and (b) equilibrium modulus for different re-polymerization time at 200°C; (e)–(f) Prediction on the storage modulus and tan δ curve of CANs at 17, 18, 19, 20, 21h' re-polymerization respectively. Red circle lines are prediction lines, black solid lines are test data lines. (For interpretation of the references to color in this figure legend, the reader is referred to the web version of this article.)

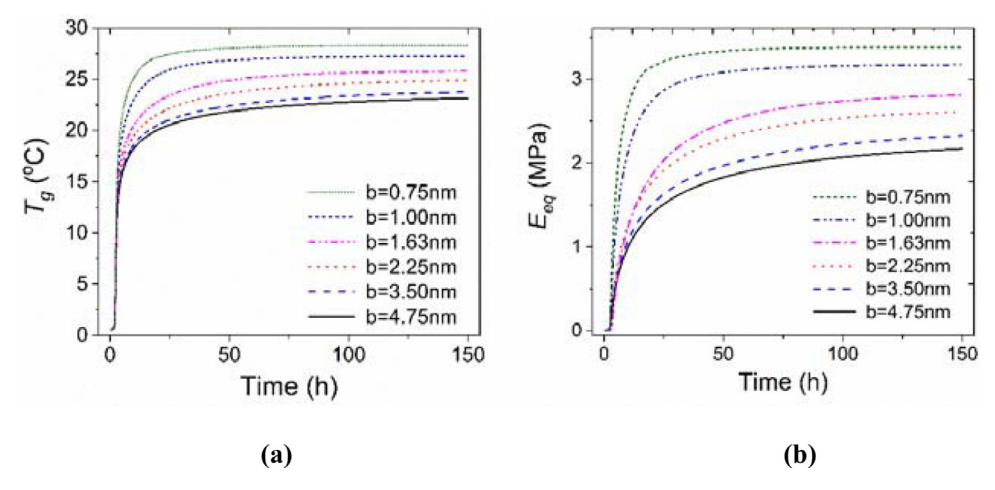


Fig. 15. Predictions on the evolution of (a) T_g and (b) equilibrium modulus for networks with different chain segment length, b.

equilibrium modulus is taken to be the storage modulus at 80°C and the network T_g is taken to be the temperature corresponding to the tan δ peak. Fig. 13(d) shows that after being heated at 200°C for 6 h, the T_g and equilibrium modulus of re-polymerized networks (26.2°C and 2.85 MPa respectively) are close to that of unprocessed epoxy (27°C and 3.21 MPa, respectively), which suggests a nearly completed reaction.

The evolutions of network equilibrium modulus and T_g during the re-polymerization can be precisely predicted by the model (Fig. 14(a) and (b)). It shows that at each temperature, the increment of T_g and rubbery moduli of recycled epoxy is faster at the early stage of re-polymerization and then slows down due to the consumption of available sites at the tail of chain segments. A high temperature increases the rate of re-polymerization because of the promoted BERs and solvent evaporation. With sufficient time of heating, the T_g and rubbery moduli at low temperature (160°C) still tends to reach the same level as those of unprocessed epoxy.

4.6. Parametric studies on the material and processing conditions

Based on the developed chemomechanics theory, parametric studies are performed to uncover the relationships between material properties, processing conditions, and recycling speed. In the first group of predictions, the average monomer length, b, was varied between 0.75 and 4.75 nm to represent that the epoxy networks were fabricated with different crosslinking densities. With the same segment number (N) between two crosslinkers, a smaller b value is corresponding to a short distance between crosslinking sites and a higher network crosslinking density. The evolution of network T_g and equilibrium modulus with different crosslinking densities are shown in Fig. 15, where the ultimate equilibrium modulus and T_g are in a linear relation with the crosslinking density. It is seen that a CAN with higher network crosslinking density

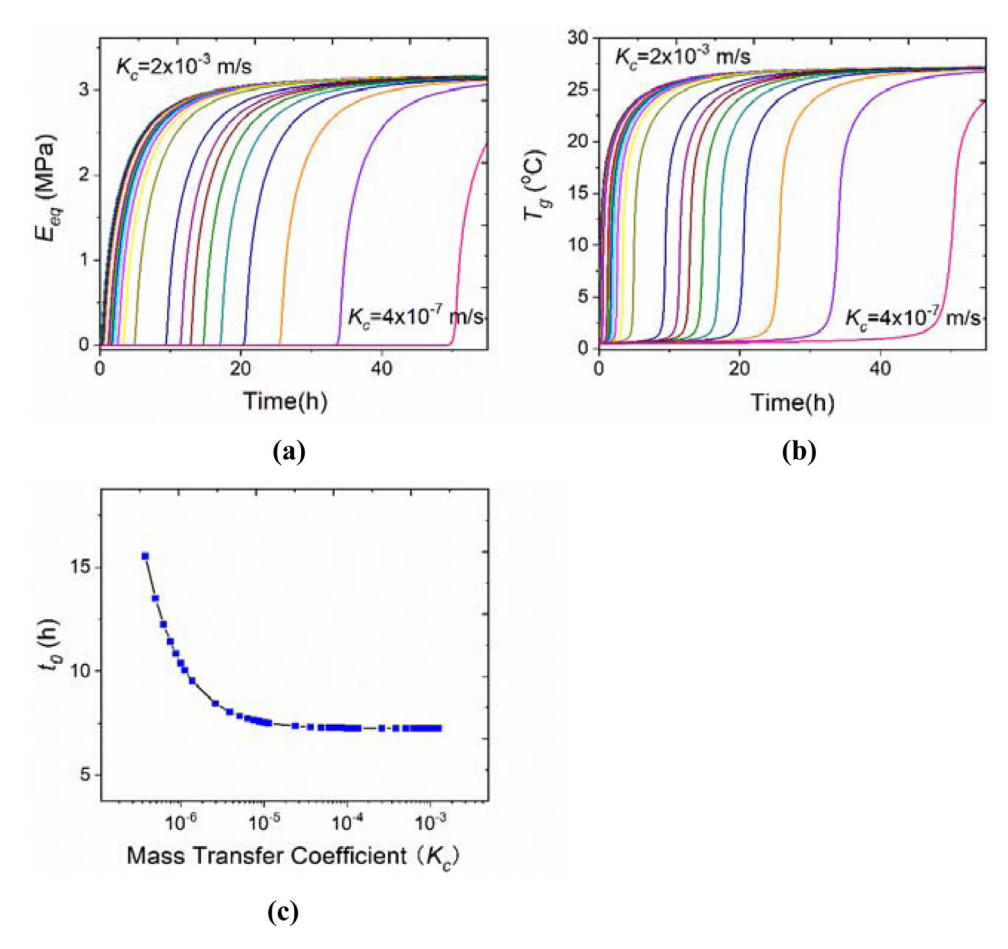


Fig. 16. Predictions on the evolution of (a) T_g and (b) equilibrium modulus with different evaporation mass transfer coefficients, K_c . (c) The repolymerization time as a function of evaporation rate.

re-polymerizes faster at the same temperature (200° C). For example, in Fig. 15(b), the re-polymerization time is taken to be the time point when the network T_g reaches 90% of the ultimate value. It decreases from 42 h to 6.2 h when the monomer length is decreased from 4.75 to 0.75 nm. For a CAN polymer with higher crosslinking density, the polymer solution contains shorter segments after decomposition, which diffuse faster for chain connection reactions, leading to a higher rate of network re-polymerization.

The choice of alcohol solvent also affects the recycling efficiency of CANs. Here, we assume that the different solvents have the same BER reactivity but different molecular weights and evaporation rates. Fig. 16(a) and(b) shows the evolution of network T_g and equilibrium modulus at 200°C when the mass transfer coefficient of solvent evaporation (K_c) varies between 4×10^{-7} and 2×10^{-3} m/s (a lower mass transfer coefficient suggests lower evaporation rate of solvent). The re-polymerization time, t_0 , is defined to be the heating time when the network T_g reaches 90% of its final value. t_0 is plotted in Fig. 16(c) as a function of the mass transfer coefficient. The results show that using an alcohol solvent with a lower evaporation rate (i.e. a higher boiling point) leads to slower re-polymerization. This is because the excessive solvent molecules accumulated in the system suppress the chain connection reaction and thus the overall re-polymerization process. The recycling efficiency can be therefore promoted by using more volatile solvent or applying processing conditions to encourage solvent evaporation (e.g. applying vacuum condition, blowing air on the sample surface). On the other hand, Fig. 16(c) reveals that the re-polymerization time does not keep decreasing with the solvent evaporation rate. It tends to saturate at 7.1 h when the mass transfer coefficient is above ~2 × 10⁻⁵ m/s. For such cases, while the solvent molecules can easily evaporate from the system, the overall re-polymerization process is still limited by the BER kinetics at a given temperature.

The type and content of BER catalyst in CANs is another parameter that affects the recycling rate. Increasing the catalyst content or using organic catalyst will reduce the energy barrier for BERs within the network. In the parametric studies, the BER activation energy, E_{ab} , was set to decrease from 23.2 to 0.15 kJ/mol to represent the increasing catalyst content. The evolutions of network T_g and equilibrium modulus at 200°C are shown in Fig. 17(a) and (b). The re-polymerization time, t_0 , is summarized in Fig. 17(c) as a function of activation energy. With more BER catalyst presents in the network, the energy

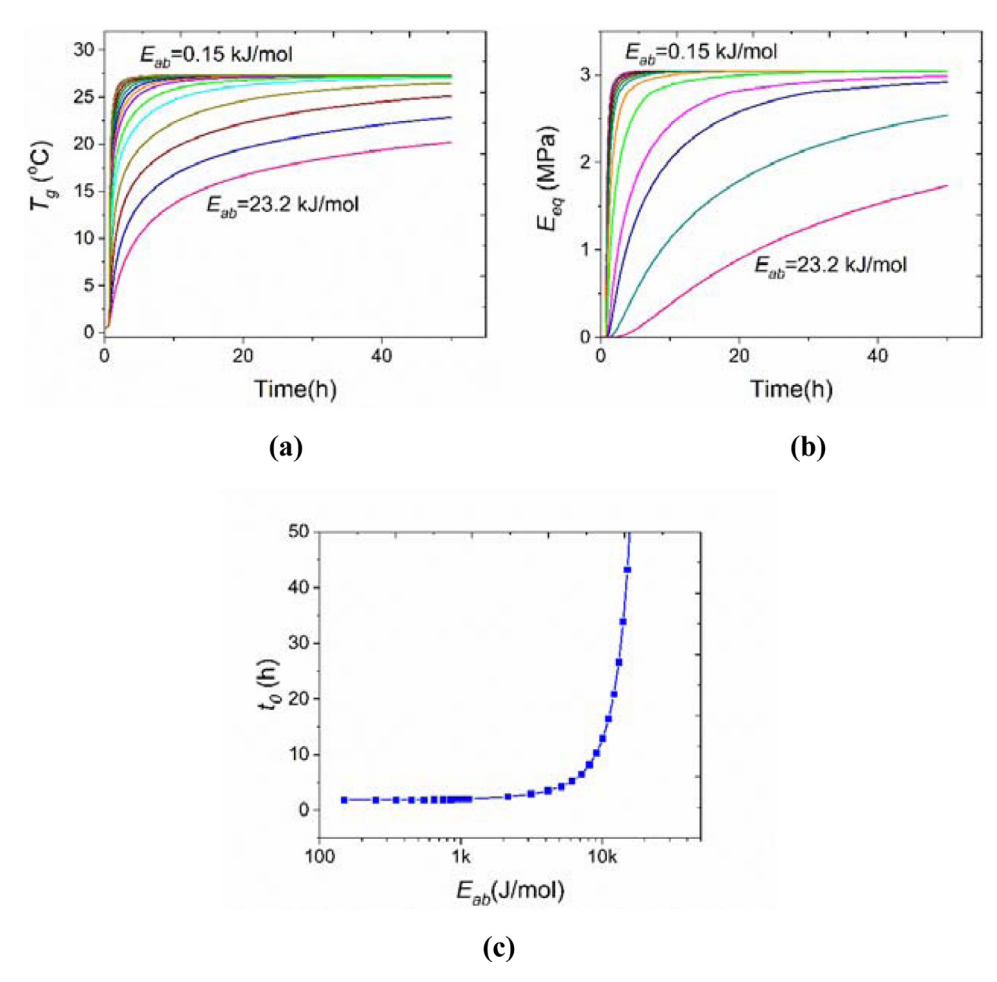


Fig. 17. Predictions on the evolution of **(a)** T_g and **(b)** equilibrium modulus with different BER energy barrier. **(c)** The re-polymerization time as a function of BER energy barrier.

barrier for the exchange reaction is lower, which greatly promotes the rate of chain connection reaction. However, the overall re-polymerization time is still limited by the solvent evaporation rate. As shown in Fig. 17(c), t_0 decreases from 66 to 6.1 h when the BER activation energy is below ~1.23 kJ/mol. Further decreasing the activation energy does not noticeably promote the re-polymerization rate because the solvent generation rate is greater than the evaporation rate, and excessive solvent molecules within the system tend to suppress the chain connection reaction.

5. Conclusion

In this paper, a multiscale chemomechanics modeling framework is developed to investigate the mechanics and physics of the solvent-assisted recycling process of thermosets. In the microscale, the chemical reaction rate is formulated by considering the diffusivity and relative distance among reactive sites. Statistical analysis is performed to determine the content and length distribution of chain segments. The conversion ratio of the functional group during the re-polymerization is used to characterize the degree of curing, which is incorporated into the continuum-level model to capture the evolution of volume shrinkage, viscosity, and network glass transition behavior. The model shows close predictions on the experimental results. Since the presented theory is based on the physics-based constitutive relations, it provides valuable insights to understand the influencing mechanisms of different material and processing conditions. For example, thermoset with a higher crosslinking density re-polymerizes faster due to the fast chain connection reactions among short segments. The overall recycling efficiency can be promoted by selecting processing conditions to increase the solvent evaporation rate and BER kinetics. These fundamental findings and the developed computational tool in this paper will pave the road for the immediate engineering applications of the green and sustainable recycling method of thermosets. They also provide a foundation for our following study on the recycling of thick thermosets involving the diffusion-reaction problems and the evolution of residual stress during the recycling of thermosets and composites.

Declaration of Competing Interest

The authors declare that they have no known competing financial interests or personal relationships that could have appeared to influence the work reported in this paper.

CRediT authorship contribution statement

Xiaojuan Shi: Software, Formal analysis, Investigation, Writing - original draft, Visualization. **Drake Soule:** Investigation, Formal analysis, Visualization. **Yiqi Mao:** Investigation, Visualization. **Christopher Yakacki:** Validation, Funding acquisition. **Haibao Lu:** Validation, Writing - review & editing. **Kai Yu:** Conceptualization, Methodology, Writing - review & editing, Supervision, Project administration, Funding acquisition.

Acknowledgments

K.Y. and C.Y. acknowledge the support from the National Science Foundation (grant CMMI-1901807).

Supplementary materials

Supplementary material associated with this article can be found, in the online version, at doi:10.1016/j.jmps.2020. 103918.

References

Adolf, D., Martin, J.E., Wilcoxon, J.P., 1990. Evolution of structure and viscoelasticity in an epoxy near the sol-gel transition. Macromolecules 23 (2), 527–531. Adzima, B.J., Aguirre, H.A., Kloxin, C.J., Scott, T.F., Bowman, C.N., 2008. Rheological and chemical analysis of reverse gelation in a covalently cross-linked Diels—Alder polymer network. Macromolecules 41 (23), 9112–9117.

Atai, M., Watts, D.C., 2006. A new kinetic model for the photopolymerization shrinkage-strain of dental composites and resin-monomers. Dent. Mater. 22 (8), 785–791.

Bowman, C.N., Kloxin, C.J., 2012. Covalent adaptable networks: reversible bond structures incorporated in polymer networks. Angew. Chem. Int. Ed. 51 (18), 4272–4274

Buback, M., Huckestein, B., Russell, G.T., 1994. Modeling of termination in intermediate and high conversion free-radical polymerizations. Macromol. Chem. Phys. 195 (2), 539–554.

Chandrasekhar, S., 1943. Stochastic problems in physics and astronomy. Rev. Mod. Phys. 15, 1-89.

Chen, X., Wudl, F., Mal, A.K., Shen, H., Nutt, S.R., 2003. New thermally remendable highly cross-linked polymeric materials. Macromolecules 36 (6), 1802–1807.

Chen, X.X., Dam, M.A., Ono, K., Mal, A., Shen, H.B., Nutt, S.R., Sheran, K., Wudl, F., 2002. A thermally re-mendable cross-linked polymeric material. Science 295 (5560), 1698–1702.

Chen, Y.C., Lagoudas, D.C., 2008. A constitutive theory for shape memory polymers. Part II-A linearized model for small deformations. J. Mech. Phys. Solids 56 (5), 1766–1778.

Conroy, A., Halliwell, S., Reynolds, T., 2006. Composite recycling in the construction industry. Compos. A: Appl. Sci. Manuf. 37 (8), 1216-1222.

Daoud, M., 2000. Viscoelasticity near the sol-gel transition. Macromolecules 33 (8), 3019-3022.

Degennes, P., Gennes, P., 1979. Scaling Concepts in Polymer Physics, 1st edition Cornell University Press.

Degennes, P.G., 1982. Kinetics of diffusion-controlled processes in dense polymer systems 1. Non-entangled regimes. J. Chem. Phys. 76 (6), 3316-3321.

Dewaele, M., Truffier-Boutry, D., Devaux, J., Leloup, G., 2006. Volume contraction in photocured dental resins: the shrinkage-conversion relationship revisited. Dent. Mater. 22 (4), 359–365.

Dewaele, M., Truffier-Boutry, D., Devaux, J., Leloupa, G., 2006. Volume contraction in photocured dental resins: the shrinkage-conversion relationship revisited. Dent. Mater. 22 (4), 359–365.

Di Marzio, E.A., Yang, A.J., 1997. Configurational entropy approach to the kinetics of glasses. J. Res. Natl. Inst. Stand. Technol. 102 (2), 135.

Diani, J., Gilormini, P., Fredy, C., Rousseau, I., 2012. Predicting thermal shape memory of crosslinked polymer networks from linear viscoelasticity. Int. J. Solids Struct. 49 (5), 793–799.

DiBenedetto, A., 1987. Prediction of the glass transition temperature of polymers: a model based on the principle of corresponding states. J. Polym. Sci. B: Polym. Phys. 25 (9), 1949–1969.

Dickey, M.D., Willson, C.G., 2006. Kinetic parameters for step and flash imprint lithography photopolymerization. AiChE J. 52 (2), 777-784.

Einstein, A., 1905. Über die von der molekularkinetischen theorie der wärme geforderte bewegung von in ruhenden flüssigkeiten suspendierten teilchen" [On the movement of small particles suspended in stationary liquids required by the molecular-kinetic theory of heat]. Ann. Phys. 322 (8), 549–560 (in German).

Es-haghi, S.S., Cakmak, M., 2015. On the thermal diffusion in polymer solutions: case study on bicomponent film drying. Polymer 79, 110-118.

Gan, S., Seferis, J., Prime, R., 1991. A viscoelastic description of the glass transition-conversion relationship for reactive polymers. J. Therm. Anal. 37 (3), 463–478.

Ge, Q., Westbrook, K.K., Mather, P.T., Dunn, M.L., Qi, H.J., 2013. Thermomechanical behavior of a two-way shape memory composite actuator. Smart Mater. Struct. 22 (5).

Gu, J.P., Leng, J.S., Sun, H.Y., 2017. A constitutive model for amorphous shape memory polymers based on thermodynamics with internal state variables. Mech. Mater. 111, 1–14.

Hanzon, D., He, X., Yang, H., Shi, Q., Yu, K., 2017. Creep-induced anisotropy in covalent adaptable network polymers. Soft Matter doi:10.1039/C7SM01174A. Hanzon, D.W., Lu, H.B., Yakacki, C.M., Yu, K., 2019. Influence of mechanically-induced dilatation on the shape memory behavior of amorphous polymers at large deformation. Mech. Time-Depend. Mater. 23 (1), 1–21.

Hartt, G. N. and D. P. Carey (1992). Economics of recycling thermosets, SAE Technical Paper.

He, X., Hanzon, D.W., Yu, K., 2018. Cyclic welding behavior of covalent adaptable network polymers. J. Polym. Sci. B - Polym. Phys. 56 (5), 402-413.

He, X., Lei, Z., Zhang, W., Yu, K., 2019. Recyclable 3D printing of polyimine-based covalent adaptable network polymers. 3D Print. Addit. Manuf. 6 (1), 31–39. Johnson, L.M., Ledet, E., Huffman, N.D., Swarner, S.L., Shepherd, S.D., Durham, P.G., Rothrock, G.D., 2015. Controlled degradation of disulfide-based epoxy thermosets for extreme environments. Polymer 64, 84–92.

Kim, J.H., Kang, T.J., Yu, W.R., 2010. Thermo-mechanical constitutive modeling of shape memory polyurethanes using a phenomenological approach. Int. J. Plasti. 26 (2), 204–218.

Kloxin, C.J., Scott, T.F., Adzima, B.J., Bowman, C.N., 2010. Covalent adaptable networks (CANs): a unique paradigm in cross-linked polymers. Macromolecules 43 (6), 2643-2653.

Kouparitsas, C., Kartalis, C., Varelidis, P., Tsenoglou, C., Papaspyrides, C., 2002. Recycling of the fibrous fraction of reinforced thermoset composites. Polym. Compos. 23 (4), 682-689.

Lee, J.H., Prud'homme, R.K., Aksay, I.A., 2001. Cure depth in photopolymerization: experiments and theory. J. Mater. Res. 16 (12), 3536-3544.

Li, Y.X., Liu, Z.S., 2018. A novel constitutive model of shape memory polymers combining phase transition and viscoelasticity. Polymer 143, 298-308.

Long, K.N., Scott, T.F., Qi, H.J., Bowman, C.N., Dunn, M.L., 2009. Photomechanics of light-activated polymers. J. Mech. Phys. Solids 57 (7), 1103-1121.

Long, R., Qi, H.J., Dunn, M.L., 2013. Modeling the mechanics of covalently adaptable polymer networks with temperature-dependent bond exchange reactions. Soft Matter 9 (15), 4083-4096.

Luo, C., Lei, Z., Mao, Y., Shi, X., Zhang, W., Yu, K., 2018. Chemomechanics in the moisture-induced malleability of polyimine-based covalent adaptable networks. Macromolecules 51 (23), 9825-9838.

Luo, C., Shi, X., Lei, Z., Zhu, C., Zhang, W., Yu, K., 2018. Effects of bond exchange reactions and relaxation of polymer chains on the thermomechanical behaviors of covalent adaptable network polymers. Polymer 153 (26), 43-51.

Luo, C., Zhang, B., Zhang, W., Yuan, C., Dunn, M., Ge, O., Yu, K., 2019. Chemomechanics of dual-stage reprocessable thermosets. J. Mech. Phys. Solids 126,

Luzuriaga, A.R.D., Martin, R., Markaide, N., Rekondo, A., Cabañero, G., Odriozola, J.R.A.I., 2016. Epoxy resin with exchangeable disulfide crosslinks to obtain reprocessable, repairable and recyclable fiber-reinforced thermoset composites. Mater. Horiz. 3, 241-247.

Montarnal, D., Capelot, M., Tournilhac, F., Leibler, L., 2011. Silica-like malleable materials from permanent organic networks. Science 334 (6058), 965-968. Nguyen, T.D., Yakacki, C.M., Brahmbhatt, P.D., Chambers, M.L., 2010. Modeling the relaxation mechanisms of amorphous shape memory polymers. Adv. Mater. 22 (31), 3411-3423.

Nielsen, L.E., 1969. Cross-linking-effect on physical properties of polymers. J. Macromol. Sci. Part C3 (1), 69-103.

O'Connell, P.A., McKenna, G.B., 1999. Arrhenius-type temperature dependence of the segmental relaxation below T-g. J. Chem. Phys. 110 (22), 11054-11060. Ogi, K., Nishikawa, T., Okano, Y., Taketa, I., 2007. Mechanical properties of ABS resin reinforced with recycled CFRP. Adv. Compos. Mater. 16 (2), 181-194. Palmer, I., Ghita, O., Savage, L., Evans, K., 2009. Successful closed-loop recycling of thermoset composites. Compos. A: Appl. Sci. Manuf. 40 (4), 490-498.

Pan, Z.Z., Zhou, Y., Zhang, N., Liu, Z.S., 2018. A modified phase-based constitutive model for shape memory polymers. Polym. Int. 67 (12), 1677-1683.

Park, H.Y., Kloxin, C.J., Scott, T.F., Bowman, C.N., 2010. Stress relaxation by addition-fragmentation chain transfer in highly cross-linked thiol-yne networks. Macromolecules 43 (24), 10188-10190.

Pickering, S.J., 2006. Recycling technologies for thermoset composite materials—current status. Compos. A: Appl. Sci. Manuf. 37 (8), 1206-1215.

Qi, H.J., Nguyen, T.D., Castro, F., Yakacki, C.M., Shandas, R., 2008. Finite deformation thermo-mechanical behavior of thermally induced shape memory polymers. J. Mech. Phys. Solids 56 (5), 1730–1751.

Rubinstein, M., Colby, R.H., 2003. Polymer Physics. Oxford University Press, New York.

Rubinstein, M., Colby, R.H., 2003. Polymer Physics. Oxford University Press, Oxford, New York.

Rudin, A., Choi, P., 2013. Diffusion in polymers. In: The Elements of Polymer Science & Engineering, pp. 275-304.

Saroso, H., 2016. Study on reaction kinetics transesterification coconut oil by using the catalyst NaOH PLUG flow reactor (PFR). Int. J. Eng. Innov. Res. 5 (3),

Scott, T.F., Draughon, R.B., Bowman, C.N., 2006. Actuation in crosslinked polymers via photoinduced stress relaxation. Adv. Mater. 18 (16), 2128-2132.

Scott, T.F., Schneider, A.D., Cook, W.D., Bowman, C.N., 2005. Photoinduced plasticity in cross-linked polymers. Science 308 (5728), 1615-1617.

Sherrod, P. H. (2000). "Nonlinear regression analysis program, NLREG Version 5.0." from http://www.nlreg.com/.

Shi, Q., Yu, K., Kuang, X., Mu, X.M., Dunn, C.K., Dunn, M.L., Wang, T.J., Qi, H.J., 2017. Recyclable 3D printing of vitrimer epoxy. Mater. Horiz. 4 (4), 598-607. Shi, x., Luo, C., Lv, H., Yu, K., 2018. Primary recycling of anhydride-cured engineering epoxy using alcohol solvent. Polym. Eng. Sci. 59 (S2), E111-E119.

Srivastava, V., Chester, S.A., Anand, L., 2010. Thermally actuated shape-memory polymers: experiments, theory, and numerical simulations. J. Mech. Phys. Solids 58 (8), 1100-1124.

Tasdelen, M.A., 2011. Diels-Alder "click" reactions: recent applications in polymer and material science. Polym. Chem. 2 (10), 2133-2145.

Taynton, P., Ni, H., Zhu, C., Yu, K., Loob, S., Jin, Y., Qi, H.J., Zhang, W., 2016. Repairable woven carbon fiber composites with full recyclability enabled by malleable polyimine networks. Adv. Mater. 28 (15), 2904-2909.

Taynton, P., Ni, H.G., Zhu, C.P., Yu, K., Loob, S., Jin, Y.H., Qi, H.J., Zhang, W., 2016. Repairable woven carbon fiber composites with full recyclability enabled by malleable polyimine networks. Adv. Mater. 28 (15), 2904-2909.

Taynton, P., Yu, K., Shoemaker, R.K., Jin, Y.H., Qi, H.J., Zhang, W., 2014. Heat- or water-driven malleability in a highly recyclable covalent network polymer. Adva. Mater. 26 (23), 3938-3942.

Watts, D., Silikas, N., 2005. In situ photo-polymerisation and polymerisation-shrinkage phenomena. Dent. Hard Tissues Bond. 123-154.

Westbrook, K.K., Parakh, V., Chung, T., Mather, P.T., Wan, L.C., Dunn, M.L., Qi, H.J., 2010. Constitutive modeling of shape memory effects in semicrystalline polymers with stretch induced crystallization. J. Eng. Mater. Technol.-Trans. ASME 132 (4).

Williams, M.L., Landel, R.F., Ferry, J.D., 1955. Temperature dependence of relaxation mechanisms in amorphous polymers and other glass-forming liquids. Phys. Rev. 98 (5) 1549-1549.

Williams, M.L., Landel, R.F., Ferry, J.D., 1955. The temperature dependence of relaxation mechanisms in amorphous polymers and other glass-forming liquids. I. Am. Chem. Soc. 77 (14), 3701-3707.

Wojtecki, R.J., Meador, M.A., Rowan, S.J., 2011. Using the dynamic bond to access macroscopically responsive structurally dynamic polymers. Nat. Mater. 10 (1), 14.

Xu, S., Liu, Z.S., 2019. A nonequilibrium thermodynamics approach to the transient properties of hydrogels. J. Mech. Phys. Solids 127, 94-110.

Yang, O.X., Li, G.O., 2016. Temperature and rate dependent thermomechanical modeling of shape memory polymers with physics based phase evolution law. Int. J. Plast. 80, 168-186.

Yu, K., Li, H., McClung, A.J.W., Tandon, G.P., Baur, J.W., Qi, H.J., 2016. Cyclic behaviors of amorphous shape memory polymers. Soft Matter 12 (13), 3234-3245. Yu, K., Qi, G., Qi, H.J., 2014. Reduced time as a unified parameter determining fixity and free recovery of shape memory polymers. Nat. Commun. 5, 3066.

Yu, K., Shi, Q., Dunn, M.L., Wang, T.J., Qi, H.J., 2016. Carbon fiber reinforced thermoset composite with near 100% recyclability. Adv. Functi. Mater. 26 (33), 6098-6106.

Yu, K., Shi, Q., Li, H., Jabour, J., Yang, H., Dunn, M.L., Wang, T., Qi, H.J., 2016. Interfacial welding of dynamic covalent network polymers. J. Mech. Phys. Solids 94, 1-17.

Yu, K., Taynton, P., Zhang, W., Dunn, M.L., Qi, H.J., 2014. Influence of stoichiometry on the glass transition and bond exchange reactions in epoxy thermoset polymers. RSC Adv. 4 (89), 48682-48690.

Yu, K., Taynton, P., Zhang, W., Dunn, M.L., Qi, H.J., 2014. Reprocessing and recycling of thermosetting polymers based on bond exchange reactions. RSC Adv. 4 (20), 10108-10117,

Yu, K., Xie, T., Leng, J., Ding, Y., Qi, H.J., 2012. Mechanisms of multi-shape memory effects and associated energy release in shape memory polymers. Soft Matter 8 (20), 5687-5695.

Yu, K., Yang, H., Dao, B.H., Shi, Q., Yakacki, C.M., 2017. Dissolution of covalent adaptable network polymers in organic solvent. J. Mech. Phys. Solids 109, 78-94

Zhang, Y., Broekhuis, A.A., Picchioni, F., 2009. Thermally self-healing polymeric materials: the next step to recycling thermoset polymers? Macromolecules 42 (6), 1906-1912.